Waveform tomography based on local image correlations

Francesco Perrone and Paul Sava, Center for Wave Phenomena, Colorado School of Mines*

SUMMARY

Common velocity analysis is based on the invariance of migrated images with respect to the experiment index (shot number, plane-wave take-off angle, etc.) or extension parameters (reflection angle, correlation lags in extended images, etc.). All the information available, i.e. the entire survey, is used for assessing the quality of the model used for imaging. This approach is effective but forces a clear separation between imaging and velocity model building. Here, we ask a complementary question: how much information about the velocity model is contained in a minimum number of images? Starting from an alternative statement of the semblance principle, we propose a measure of velocity error based on local correlations of pairs of migrated images. We design an objective function and implement a local, gradient-based optimization scheme to reconstruct the velocity model. Our methodology is "full-wave" because it is not based on a linearization of the imaging operator (in contrast with linearized wave-equation migration velocity analysis techniques). The gradient of the objective function is computed using the adjoint-state method.

INTRODUCTION

Seismic imaging includes estimation of both the *position* of the structures responsible for the recorded data and a *model* that describes the propagation in the subsurface. The two problems are related since a model is necessary to infer the position of the reflectors. The recorded wavefields are extrapolated in the model by solving a wave equation and crosscorrelated with a synthetic source wavefield simulated in the same model (Claerbout, 1985). Under a single scattering approximation, reflectors are located where the source and receiver wavefields match in time and space. If the velocity model is inaccurate, the reflectors are positioned at incorrect locations.

Wave-equation tomography is a family of techniques that estimate the velocity model from finite bandwidth signals. The inversion is usually formulated as an optimization problem, where the correct velocity minimizes an objective function that measures the inconsistency between simulated and observed data. Full-waveform inversion (FWI) (Tarantola, 1984; Pratt, 1999; Sirgue and Pratt, 2004) addresses the estimation problem in the data space and measures the mismatch between observations and simulated data. FWI aims to reconstruct the exact model that generates the recorded data. By matching both traveltime and amplitude information, FWI allows one to achieve high-resolution results (Sirgue et al., 2010). Nonetheless, it needs a source estimate, the physics of wave propagation must be correctly modelled and a good parametrization (for example, impedance vs. velocity contrasts) is crucial (Kelly et al., 2010). Moreover, an accurate initial model is key to avoid cycle skipping and convergence to the global minumum of the objective function. Migration velocity analysis (MVA) (Fowler, 1985; Faye and Jeannot, 1986; Al-Yahya, 1989; Chavent and Jacewitz, 1995; Biondi and Sava, 1999; Sava et al., 2005; Albertin et al., 2006) defines the objective function in the image space and is based on the semblance principle (Al-Yahya, 1989). Groups of experiments and the associated images are analyzed. If the velocity model is correct, the images from different experiments must be consistent since the Earth is assumed stationary on the time scale of the seismic experiments. MVA leads to smooth objective functions and well-behaved optimization problems (Symes, 1991; Symes and Carazzone, 1991), and it is less sensitive to the initial model than FWI. On the other hand, because we lose the information about the data amplitudes, the estimated model shows lower resolution than the FWI result. MVA measures either the invariance of the migrated images in an auxiliary dimension (reflection angle, shot, etc.) (Al-Yahya, 1989; Sava and Fomel, 2003; Xie and Yang, 2008) or focusing in an extended space (Rickett and Sava, 2002; Symes, 2008; Sava and Vasconcelos, 2009). A large number of shots and good illumination are necessary to pick moveout curves or assess focusing. Moreover, because of the high memory requirement for storing the information from each experiment, only a subset of the image is considered in the evaluation of the objective function. For example, common-image gathers (CIGs) (Rickett and Sava, 2002; Yang and Sava, 2011) or common-image point (CIPs) (Sava and Vasconcelos, 2009) are computed at fixed lateral positions or picked image points along reflectors, respectively, and both methods require migration of all the shots that illuminate the location where the CIGs/-CIPs are constructed.

We propose an objective function that operates in the image space and does not need CIGs. We consider small groups of images from neighboring experiments and formulate the semblance principle in the shot-image domain, instead of the extended space at selected CIGs. We use the morphologic relationship between images from neighboring experiments to define a measure of relative shifts in the image space. This approach reduces the memory requirements and allows us to include all image points in the velocity analysis step.

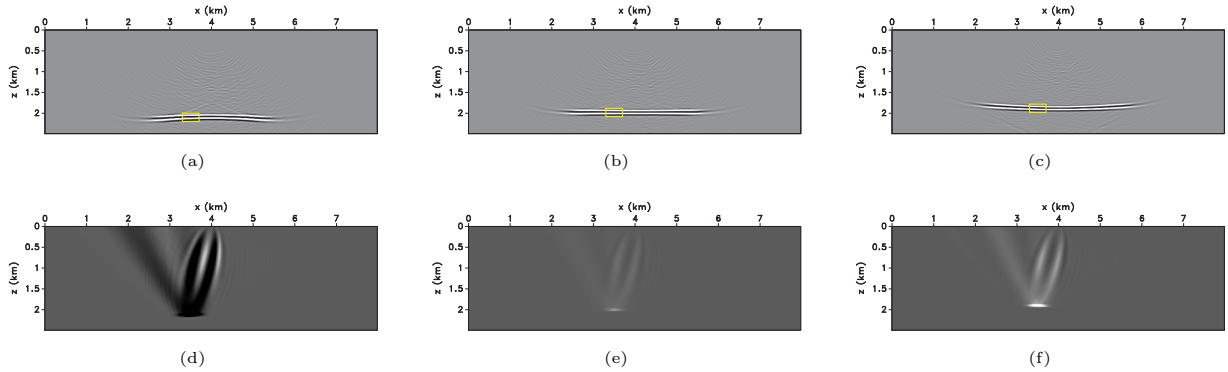

Figure 1: Images of a flat reflector obtained using a velocity model that is (a) too high, (b) correct, and (c) too too low. For each model we compute the sensitivity kernel associated with the highlighted box. Panels (d), (e), and (f) show the sensitivity kernels for the corresponding models.

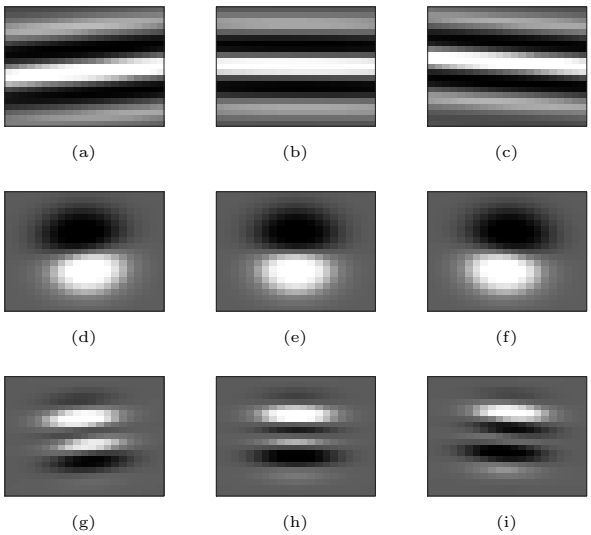

Figure 2: Local image correlations ((a), (b), and (c)), penalty operators ((d), (e), and (f)), and penalized local correlations ((g), (h), and (i)) for the box highlighted in Figure 1 and the three models (velocity too high, correct, and too low, respectively).

THEORY

MVA is based on the semblance principle (Al-Yahya, 1989): a single Earth model generates the recorded data; then, if the velocity model is correct, different experiments must produce consistent images of the reflectors. The similarity between migrated images is usually assessed through the analysis of common-image gathers (CIGs), which can be constructed in different domains (reflection angle, ray parameter, sub-surface offset, etc.) (Sava and Fomel, 2003; Shen and Symes, 2008; Xie and Yang, 2008), or extended images (EIs) (Rickett and Sava, 2002; Symes, 2008; Sava and Vasconcelos, 2009). These approached require migration of a large number of shots in order to measure moveout in the CIGs or focusing in EIs. Alternatively, we can measure the similarity of pairs of images by computing local correlations at each image point. We define the objective function

$$\mathcal{J}(m) = \frac{1}{2} \sum_i \| \sum_{\boldsymbol{\lambda}} P\left(\mathbf{x}, \boldsymbol{\lambda}\right) c_i\left(\mathbf{x}, \boldsymbol{\lambda}\right) \|^2_{\mathbf{x},\boldsymbol{\lambda}}, \qquad (1)$$

where $c_i\left(\mathbf{x}, \boldsymbol{\lambda}\right) = \int_{w(\mathbf{x})} R_{i+1}\left(\boldsymbol{\xi} - \frac{\boldsymbol{\lambda}}{2}\right) R_i\left(\boldsymbol{\xi} + \frac{\boldsymbol{\lambda}}{2}\right) d\boldsymbol{\xi}$ is the local correlation of R_i and R_{i+1} and P is a penalty operator that highlights features that are related to velocity errors. The correlations are computed in local windows $w\left(\mathbf{x}\right)$, which allow us to consider small subsets of the data. The index i spans the shots and m denotes the model. In this work, we define the objective function using pairs of shots, but we use the entire images obtained from them, instead of analyzing only sparsely selected CIGs or CIPs. The reduced input data leads to lower memory requirements with respect to other techniques based on common image-gathers or extended images. A possible alternative to measure inconsistencies between migrated images is the energy of the difference between them. Plessix (2006) uses the image difference as a regularization term for full-waveform inversion and not as a stand-alone objective function. The difference operator is a high-pass filter, enhances noise, and is sensitive to amplitude patterns. Images from different shots do not have identical amplitudes at a given spatial location because the wavefields experience different propagation paths. The bigger the separation between the shots, the higher the amplitude mismatch. The difference objective function considers this discrepancy a velocity error indicator and thus this objective function is intrinsically biased. Local correlations measure phase shifts between two images. Correlation is more robust because amplitudes are not directly used for measuring velocity errors. Nonetheless, the size of the correlation window must be such that it captures the relative shift between the two images. Local correlation in the image space is analogous to data correlation for FWI, as proposed by van Leeuwen and Mulder (2008, 2010).

We restate the semblance principle as follows: if the velocity model is correct, two images from nearby experiments constructively interfere along the direction of the reflectors (Perrone and Sava, 2012). This is equivalent to having no moveout in shot-domain CIGs (Xie and Yang, 2008). Figure 1 shows the migrated images of a horizontal reflector with three velocity models (too high (a), correct (b), and too low (c)) and the sensitivity kernels ((d), (e), and (f)) for the local window highlighted by the box. The sign of the sensitivity kernel is consistent with the velocity error. Figure 2 shows the local correlations, penalty operators, and penalized correlations for the box in Figure 1. The similarity between two images is measured by the inconsistency between the local correlation and the dip estimated from one image. If the velocity model is correct, the *maximum* of the correlation lies along the reflector slope (the central column of Figure 2); the penalized correlation is an odd function, and the stack over correlation lags is practically zero, i.e., the two image are aligned and the model is correct. If the velocity is incorrect (the first and third column of Figure 2), we observe a deviation that depends on the sign and extent of the velocity error. This deviation is measured as a mismatch between the orientation of the penalty operator (constructed from the estimated dip in the image) and of the the local correlation. The penalized correlation are not odd functions and their mean value measures the relative shift between the two images.

The penalty operator P is constructed from the estimated dip field (which depends on the model parameters as well). The dependence of P on the wavefield u can be accounted for by expressing the dip as a function of the image through gradient square tensors (van Vliet and Verbeek, 1995). This relationship is highly nonlinear and a thorough study of $\partial P/\partial u$ and its impact on the adjoint-state calculations is subject of further research.

SYNTHETIC EXAMPLES

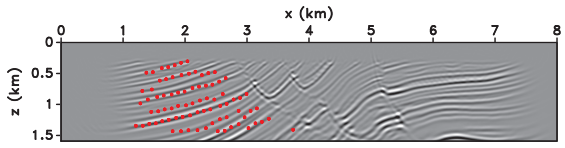

Figure 3: Picking for a single shot-image. The shot position is $x = 1.76$ km. The picks are overlaid on the complete image for the sake of clarity. The adjoint sources are computed only at the picked locations.

We run a second test using the Marmousi model. We simulate 78 shots with a finite-difference single-scattering modeling code and absorbing boundary conditions on the 4 sides of the model. The spacing between the shots is 0.08 km, and the first source is at $x = 0.96$ km; receivers are placed 0.008 km apart on the surface.

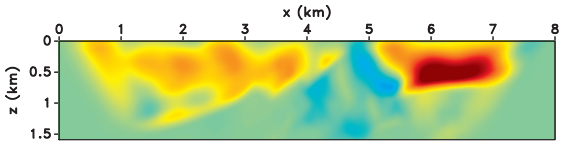

Figure 4: Gradient of the objective function for the 11 iteration.

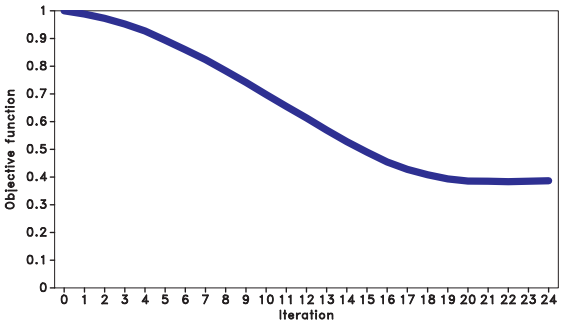

Figure 6: Objective function evolution over 24 iterations.

For the computation of the adjoint sources and then of the adjoint wavefields, we pick points along the structures in the image. Figure 3 shows the picks obtained from a particular shot (at $x = 1.76$ km). The picks are displayed on the complete image for the sake of clarity. Observe how the picks follow the main reflectors illuminated by that particular shot. By picking a limited number of image points to compute the adjoint sources we can greatly speed up the computation of the gradient of the objective function.

Figure 4 shows an example of the computed gradient of the objective function. In this case, we show the 11 iteration because the gradient clearly shows structural features in it. The more shallower and strong reflectors (about $z = 0.75$ km) clearly constrain of the velocity update and we start recovering the low slowness anomaly in the central part of the model.

The initial model is a heavily smoothed and scaled version of the original Marmousi slowness model. Figures 5(a), 5(c), and 5(e) show the initial model, migrated image, and shot-domain CIGs extracted every 1 km from $x = 0$ km, respectively. Our inversion algorithm is based on a clear and unambiguous definition of the structural features in the image. At the locations where the image has conflicting dips, the shape of the correlation panel cannot be directly related and compared with the structural information encoded in the dip field that is measured from the image itself. For this reason, we restrict the inversion to the first 1.6 km in depth, where the reflectors are more coherent. For more complicated models with conflicting dips and complicated geologic features (where there is no clear definition of the dip field), a more sophisticated design of

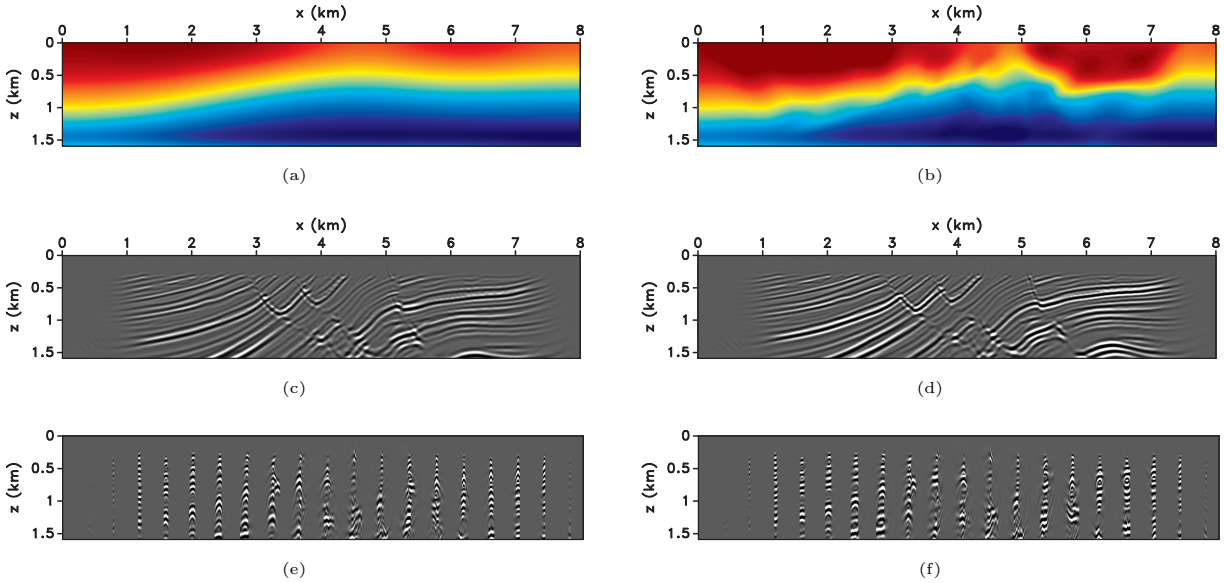

Figure 5: (a) Initial and (b) updated slowness model after 24 iterations of waveform tomography; (c) intial image and (d) migrated image with the updated model; (e) intial shot-domain CIGs and (f) CIGs with the updated model.

the penalty operator is necessary. The eigenvalues and eigenvectors of the gradient square tensors (van Vliet and Verbeek, 1995) can be used to define ellipses that, in turn, may offer a structure oriented criterion for the definition of the penalty operators.

The migrated image (Figure 5(c)) presents crossing interfaces and defocused fault planes; the shot-domain CIGs (Figure 5(e)) show variation of the depth of reflectors as a function of experiment, which indicates model inaccuracy. After 24 steepest-descent iterations, we obtain the results in Figures 5(b), 5(d), and 5(f). The interfaces are moved toward the correct position, and we observe better focusing of the fault planes. The shot-domain CIGs in Figure 5(f) show flatter events, which indicate a more kinematically accurate model, and overall more energy is mapped in the image. The image does not constrain the velocity update in the water layer since a strong water bottom reflection is missing and this explains the smearing of the update in the shallower part of the model.

Figure 6 shows the evolution of the objective function with iterations. The smoothness of the objective function is due to the small step used for implementing the line search in the steepest-descent algorithm. The nonzero value at convergence after 24 iterations is mainly due to the fact that, at this stage, *all* points in the image contribute to the computation of the objective function, also points in complex areas and on crossing reflection events, where our assumptions for measuring velocity model errors fail.

CONCLUSIONS

We present an approach to waveform tomography based on the semblance principle in the shot-image domain. We define an objective function using appropriately penalized local image correlations that measure the relative shift between two images obtained from nearby experiments; the penalty operator enhances the mismatch between the structural information (the orientation of the reflector) and the shift between two images. The gradient of the objective function with respect to the model is computed with the adjoint-state method, which makes our technique a close relative to the more conventional full waveform inversion. Inversion on a simple synthetic and the Marmousi model shows the ability of our strategy to correct model errors.

ACKNOWLEDGMENTS

We would like to thank eni E&P for the permission to publish this work and Nicola Bienati for the valuable conversations on tomography and inversion. The reproducible numerical examples in this paper use the Madagascar open-source software package freely available from http://www.reproducibility.org. This research was supported in part by the Golden Energy Computing Organization at the Colorado School of Mines using resources acquired with financial assistance from the National Science Foundation and the National Renewable Energy Laboratory.

REFERENCES

Al-Yahya, K., 1989, Velocity analysis by iterative profile migration: Geophysics, **54**, P. 718–729.

Albertin, U., P. Sava, J. Etgen, and M. Maharramov, 2006, Adjoint wave-equation velocity analysis: Presented at the 74th Ann. Internat. Mtg., SEG.

Biondi, B., and P. Sava, 1999, Wave-equation migration velocity analysis: Presented at the 69th Ann. Internat. Mtg., SEG.

Chavent, G., and C. A. Jacewitz, 1995, Determination of background velocities by multiple migration fitting: Geophysics, **60**, 476–490.

Claerbout, J. F., 1985, Imaging the earth's interior: Blackwell Publishing.

Faye, J.-P., and J.-P. Jeannot, 1986, Prestack migration velocity analysis from focusing depth imaging: Presented at the 56th Ann. Internat. Mtg., Soc. of Expl. Geophys.

Fowler, P., 1985, Migration velocity analysis by optimization: Technical Report 44, Stanford Exploration Project.

Kelly, S., J. R. Martinez, B. tsimelzon, and S. Crawley, 2010, A comparison of inversion results for two full-waveform methods that utilize the lowest frequencies in dual-sensor recordings: Presented at the 80th Ann. Internat. Mtg., Soc. of Expl. Geophys.

Perrone, F., and P. Sava, 2012, Wavefield tomography based on local image correlation: Presented at the 72th Ann. Internat. Mtg., European Association of Geoscientists and Engineers.

Plessix, R.-E., 2006, A review of the adjoint-state method for computing the gradient of a functional with geophysical applications: Geophys. J. Int., **167**, 495–503.

Pratt, R. G., 1999, Seismic waveform inversion in the frequency domain, part 1: Theory and verification in a physical scale model: Geophysics, **64**, 888–901.

Rickett, J., and P. Sava, 2002, Offset and angle-domain common image-point gathers for shot-profile migration: Geophysics, **67**, 883–889.

Sava, P., B. Biondi, and J. Etgen, 2005, Wave-equation migration velocity analysis by focusing diffractions and reflections: Geophysics, **70**, U19–U27.

Sava, P., and S. Fomel, 2003, Angle-domain common-image gathers by wavefield continuation methods: Geophysics, **68**, 1065–1074.

Sava, P., and I. Vasconcelos, 2009, Extended common-image-point gathers for wave-equation migration: Presented at the 71th Ann. Internat. Mtg., European Association of Geoscientists and Engineers.

Shen, P., and W. W. Symes, 2008, Automatic velocity analysis via shot profile migration: Geophysics, **73**, VE49–VE59.

Sirgue, L., O. I. Barkved, J. Dellinger, J. Etgen, U. Albertin, and J. H. Kommedal, 2010, Full waveform inversion: the next leap forward in imaging at valhall: First Break, **28**, 65–70.

Sirgue, L., and R. Pratt, 2004, Efficient waveform inversion and imaging: A strategy for selecting temporal frequencies: Geophysics, **69**, 231–248.

Symes, W. W., 1991, Layered velocity inversion: A model problem from reflection seismology problem from reflection seismology: SIAM J. on Math. Analysis, **22**, pp. 680–716.

———, 2008, Migration velocity analysis and waveform inversion: Geophysical Prospecting, **56**, 765–790.

Symes, W. W., and J. J. Carazzone, 1991, Velocity inversion by differential semblance optimization: Geophysics, **56**, 654–663.

Tarantola, A., 1984, Inversion of seismic reflection data in the acoustic approximation: Geophysics, **49**, 71–92.

van Leeuwen, T., and W. A. Mulder, 2008, Velocity analysis based on data correlation: Geophysical Prospecting, **56**, 791 – 803.

———, 2010, A correlation-based misfit criterion for wave-equation traveltime tomography: Geophys. J. Int., **182**, 1383–1394.

van Vliet, L. J., and P. W. Verbeek, 1995, Estimators for orientation and anisotropy in digitalized images: Proceedings of the first annual conference of the Advanced School for Computing and Imaging, ASCI'95, 442–450.

Xie, X. B., and H. Yang, 2008, The finite-frequency sensitivity kernel for migration residual moveout and its applications in migration velocity analysis: Geophysics, **73**, S241–S249.

Yang, T., and P. Sava, 2011, Wave-equation migration velocity analysis with time-shift imaging: Geophysical Prospecting, **59**, 635–650.